Revision 1

Amphibole fractionation and its potential redox effect on arc crust: Evidence from the Kohistan arc cumulates

Jingbo Zhang[1], Rui Wang[1,] *, Jun Hong[2]

1. State Key Laboratory of Geological Processes and Mineral Resources, Institute of Earth Sciences, China University of Geosciences, Beijing 100083, China

2. MNR Key Laboratory for the Study of Focused Magmatism and Giant Ore Deposits, Xi'an Center of Geological Survey, CGS, Xi'an 710054, China

*Corresponding author: **Rui Wang**

Institute of Earth Sciences, China University of Geoscience

29 XUEYUAN RD., Haidian District

Beijing 100083, China

Phone: (+86) 010 82323212

E-mail: rw@cugb.edu.cn

ABSTRACT

Arc magmas, a major contributor to continental crust growth, are thought to be more oxidized than mid-ocean ridge basalts as reflected by an enrichment in ferric iron relative to ferrous iron, but how arc magmas become oxidized is hotly debated. It is acknowledged that the fractionation of common Fe-rich phases (e.g., amphibole) may change the Fe valence of the derivative melt. Amphibole has Fe-rich compositions commonly found in arc systems. We present high precision (±0.01%) Fe valence data of amphibole and cumulates from the Kohistan arc determined by Mössbauer spectroscopy, and bulk cumulate $Fe^{3+}/\sum Fe$ ratios by wet chemistry. We evaluate the $Fe^{3+}/\sum Fe$ trend of Fe-rich amphibole during arc magma fractionation. Our results show that bulk $Fe^{3+}/\sum Fe$ ratio of cumulates in mature island arc settings is mainly controlled by amphibole due to its abundance and decreases (from 0.4 to 0.2) with decreasing Mg# as $Fe^{3+}/\sum Fe$ ratios decrease in amphibole (from 0.35 to 0.2). Our modeling suggests that amphibole fractionation from parental arc magmas to $Fe^{3+}/\sum Fe$ above 0.2 may lead to an increase in $Fe^{3+}/\sum Fe$ ratios of middle-late stage residual melts by 0.1-0.3, and the partitioning of ferrous Fe into amphibole increases with the evolution of arc magmas. Our findings highlight the importance of petrological processes in the magma that contribute to the production of fertile arc crust.

Keywords: amphibole, iron valence, Kohistan cumulate, redox state, porphyry deposit

INTRODUCTION

The oxidation state reflected by oxygen fugacity (fO_2) plays an important role in many physical and chemical processes including metasomatism, magma genesis, ore-forming processes and atmospheric evolution (e.g., Cottrell and Kelley, 2011; Frost and McCammon, 2008). Previous studies indicate that arc magmas are oxidized with ΔFMQ (relative to fayalite-magnetite-quartz buffer) of +0.5 to +2, and locally may be greater than +3 (Richards, 2015, and references therein). However, there is a debate on whether the oxidized nature of arc magmas is inherited from the mantle source or acquired by magmatic differentiation, crustal interaction, or degassing during magma upwelling (e.g., Bounce et al., 2014; Burgisser and Scaillet, 2007; De Hoog et al., 2004; Kelley and Cottrell, 2009; Lee et al., 2010).

Iron is the most abundant multi-valence element in magmatic systems, thus Fe-bearing minerals play an important role in modulating redox conditions. One hypothesis suggests that garnet fractionation in thick continental arcs results in the oxidation of the residual melt due to its preference for Fe^{2+} over Fe^{3+} (Tang et al., 2018, 2019a). Although garnet may crystallize at the base of mature island arcs built on crust >30 km thick, such as Talkeetna arc in south-central Alaska (Bucholz and Kelemen, 2019; Kelemen et al., 2014), its redox effect may be much less significant due to its generally low proportions in island arc cumulates. Amphibole fractionation is more common in arc systems (Davidson et al., 2007; Dessimoz et al., 2012), and amphibole-bearing cumulates are frequently observed at convergent margins (Jagoutz and Schmidt, 2012; Santana et al., 2020; Xu et al., 2019; Zhang et al., 2020; Zhu et al., 2019). Previous studies focused on the partitioning of $Fe^{3+}/\sum Fe$ [atomic $Fe^{3+}/(Fe^{3+}+Fe^{2+})$] between

synthetic amphibole and basanitic melt at 1100-1175 °C and 1.5-2.0 GPa (King et al., 2000). However, these conditions are not equivalent to those in arc magmas, and whether amphibole fractionation can control the $Fe^{3+}/\sum Fe$ of evolving arc magmas is still unclear.

The Kohistan arc in Northern Pakistan is a mature island arc with exposures of a continuous section from the lithospheric mantle through lower crustal cumulates to mid-crustal gabbros and granitoids (Dhuime et al. 2007; Jagoutz, 2014; Jagoutz and Schmidt, 2012). The cumulates represent early products of crystallization during hydrous, high-pressure fractionation starting from a mantle-derived basaltic melt (Jagoutz et al., 2011), and they have not experienced subsequent crustal processes, such as assimilation or degassing (Jagoutz and Schmidt, 2012). There is a complementary relationship between the ultramafic to mafic cumulates and shallow-level intermediate-to-felsic arc magmas, the granitoids in the Kohistan batholith can be successfully modeled by crustal fractionation of the minerals present in the cumulates (Jagoutz et al., 2009; Jagoutz, 2010). Thereby, these cumulates provide an ideal case to study the evolution of the $Fe^{3+}/\sum Fe$ ratio and potential redox state of arc magmas. In this study, we determine the $Fe^{3+}/\sum Fe$ ratio of amphibole, garnet, and bulk Kohistan cumulates to evaluate the roles of amphibole and garnet fractionation in controlling the Fe valence, and thus the redox state of a differentiating arc magma.

GEOLOGICAL SETTING AND SAMPLES

The Kohistan arc, exposed in NE Pakistan, is one of the best-preserved complete

arc sections in the geological record (Burg, 2011; Jagoutz, 2014; Jagoutz and Schmidt, 2012; Zhang et al., 2021), representing the exhumed section of a Cretaceous intraoceanic arc formed during presumably north-dipping subduction in the equatorial region of the Neo-Tethys Ocean. The former arc is now sandwiched between the Eurasian plate to the north and the Indian plate to the south; it is separated from the Eurasian margin by the Shyok (Karakoram-Kohistan) suture and from the Indian continent by the Indus suture (Fig. 1A). To the east, the Kohistan arc is separated from the Ladakh arc by the Nanga Parbat Syntaxis.

The Kohistan arc is composed of Jurassic-Cretaceous to Paleogene igneous and sedimentary rocks. In the southmost part of the Kohistan arc, the Jijal Complex represents the upper mantle to lower crust transition overlain by a thick sequence of metaplutonic and minor metavolcanic and metasedimentary rocks referred to as the Southern Amphibolites (Kamila Complex). The Chilas Complex resulted from the intra-arc extension and rifting at the base of the arc (Burg, 2011), and separates the Southern Amphibolites from the Gilgit Domain to the north, which is composed primarily of upper crustal plutonic rocks (Kohistan Batholith), volcanic and volcanoclastic rocks, and sedimentary rocks (Fig. 1A).

The Jijal complex represents the roots of the Kohistan arc. This complex is composed of a lower ultramafic section and an upper mafic section (Dhuime et al., 2007; Jagoutz et al., 2011). From the bottom to the top, the ultramafic section is subdivided into a peridotite zone, a pyroxenite zone, and a garnetite plus hornblendite zone (Fig. 1B). The mafic section (garnet gabbro zone) is dominated by garnet-bearing gabbroic

rocks, with lenses of hornblendites enclosed in the garnet gabbros.

Amphibole-bearing samples were collected from the Jijal complex and comprise both hornblendite and garnet hornblendite. For comparison, some amphibole-free samples (garnet pyroxenite and pyroxene garnetite) were also analyzed. The composition of minerals in each sample are listed in Table 1. The amphibole-bearing samples characterized by magmatic features and cumulate textures are composed of euhedral amphibole and garnet (Figs. 2A and B). Similar characteristics also exist in amphibole-free samples that are mainly composed of clinopyroxene and garnet (Figs. 2C and D). Some samples contain small amounts of plagioclase (≤10 vol%) and trace magnetite (<1 vol%).

ANALYTICAL METHODS

Whole-rock major elements

Major element analyses of whole-rock samples were conducted at the Wuhan Sample Solution Analytical Technology Co., Ltd. Fresh chips of whole-rock samples were washed using distilled water, and then powdered to 200 mesh using a tungsten carbide ball mill. Major element concentrations were determined with an X-ray fluorescence (XRF) spectrometer (Primus II, Rigaku, Japan), with analytical uncertainties lower than 2%. The FeO contents were determined by the potassium dichromate titration (wet chemistry).

Mössbauer spectroscopy

The $Fe^{3+}/\sum Fe$ of garnet and amphibole were determined by Mössbauer

spectroscopy at the Dalian Institute of Chemical Physics, Chinese Academy of Sciences using hand-picked, optically pure mineral grains. The amount of sample material was adjusted to maintain a sample thickness of 10 mg Fe cm^{-1}, which served to minimize saturation effects. The room temperature ^{57}Fe Mössbauer spectra of the selected PB/TiO_2 NPs with a molar ratio of 1:60 was recorded under various simulated conditions by using a Topologic 500A spectrometer and a proportional counter. ^{57}Co (Rh), moving with a constant acceleration mode, was used as the γ-ray radioactive source. The velocity was calibrated by a standard α-Fe foil. The collection time for each sample was 24 hours. Fits to Mössbauer spectra were performed using Mosswinn software (Klencsár et al., 1996), and constraints on isomer shift were used for the Fe^{3+} doublet, whose value was usually less than 0.5. This observation is consistent with the peak width of Fe^{3+} doublet constrained to 0.4 mm s^{-1} (Aulbach et al., 2017). The calculated $Fe^{3+}/\sum Fe$ values have absolute uncertainties of ±0.01%.

RESULTS

Our samples of hornblendite, garnet hornblendite, garnet pyroxenite and pyroxene garnetite have SiO_2 contents of 40.42 to 52.20 wt%, MgO contents of 4.65 to 15.33 wt%, $Fe_2O_3^T$ contents of 10.90 to 15.60 wt%, and FeO contents determined by wet chemistry of 6.50 to 12.50 wt%. The whole-rock $Fe^{3+}/\sum Fe$ ratios of all samples vary from 0.15 to 0.42 (Table 1).

In order to cover the maximum range, we selected samples with the broadest range of bulk Mg# in which to analyze the $Fe^{3+}/\sum Fe$ ratios. Amphiboles from samples

18JL023, 18JL029, and 18JL040, and garnets from samples 18JL019, 18JL021, 18JL023, and 18JL040 were separated for analysis. $Fe^{3+}/\sum Fe$ ratios of garnet and amphibole from the Kohistan Jijal complex measured by Mössbauer spectroscopy vary from 0.071 to 0.084, and 0.23 to 0.35, respectively. Corresponding spectra and fits are shown in Figure 3, and the fitting parameters are listed in Table S1. The results demonstrate that the $Fe^{3+}/\sum Fe$ ratios of both bulk cumulates and amphiboles decrease with decreasing Mg#. In contrast, there is no correlation between the $Fe^{3+}/\sum Fe$ ratios in garnets and their Mg#. In addition, the $Fe^{3+}/\sum Fe$ ratio of amphibole-free samples is significantly lower than that of amphibole-bearing samples (Fig. 4).

DISCUSSION

Cumulate origin for Jijal Complex samples

Several lines of evidence indicate that Kohistan Jijal complex samples formed by direct crystal accumulation, and are thus of cumulate origins. Firstly, the samples are characterized by magmatic features and cumulate textures, and are composed of euhedral pyroxenes, garnet, and amphiboles (Fig. 2). Secondly, their major element compositions (low SiO_2, high MgO and FeO^T contents) are similar to previously reported typical cumulates trends from the Kohistan arc (Jagoutz, 2014) and Arizona xenoliths (Chen et al., 2020; Erdman et al., 2016), and they are complementary to typical calc-alkaline arc magmas such as those from Honshu, Luzon, Kohistan-Ladakh and Gangdese (Fig. 5B). Finally, all cumulate samples fall on the Z-shaped cumulate line derived from experimental studies of hydrous differentiation of basaltic melts under

10 kbar (Fig. 5A) (Müntener and Ulmer, 2018). Different segments of the Z-shaped trend are controlled by variable mineral assemblages and proportions. The first segment is mainly caused by the fractionation of olivine and pyroxene, the second segment by silica-poor minerals such as garnet, Fe-Ti oxides and hornblende, and the third segment by the reappearance of pyroxene in gabbroic rocks (Jagoutz et al., 2011). These geochemical characteristics are consistent with our observed cumulate sequence.

The role of amphibole fractionation in controlling $Fe^{3+}/\sum Fe$

Iron is the most abundant variable valence element in the crust and mantle, and it exists in ferromagnesian silicates or Fe oxides in the form of Fe^{2+} and Fe^{3+}, therefore fluctuation in the $Fe^{3+}/\sum Fe$ ratio is mainly controlled by the behavior of Fe-rich minerals. To investigate the evolution of $Fe^{3+}/\sum Fe$ in the Kohistan arc magma, a compilation from the GEOROC database was assembled. We selected both volcanic rocks and plutonic rocks that involved little contamination and thus should reflect magmatic features and trends (Jagoutz and Schmidt, 2012), and for which both Fe_2O_3 and FeO were reported so that the $Fe^{3+}/\sum Fe$ could be calculated. The results show that $Fe^{3+}/\sum Fe$ ratios of Kohistan-Ladakh arc magmas increase with decreasing Mg# (Fig. 6A). The weakly negative correlation between Dy/Yb and SiO_2 indicates that the Kohistan arc magma experienced amphibole fractionation in the deep crust (Fig. 6B; Davidson et al., 2007). It is consistent with the observation that amphibole-bearing cumulates are widely distributed in the Kohistan arc root (Jagoutz et al., 2011; Jagoutz and Schmidt, 2012). In addition, the analytical results show that bulk amphibole-rich

cumulates possess parallel $Fe^{3+}/\sum Fe$ ratios to amphiboles, and significantly higher ratios than amphibole-free cumulates (Fig. 4). It also suggests that amphibole crystallized in deep crustal levels at high pressure (pressure data see Jagoutz and Schmidt, 2012) may play an important role in controlling $Fe^{3+}/\sum Fe$ ratio. Due to the intra-oceanic nature of the Kohistan arc, data form the modern Tonga intra-oceanic island arc were also compiled for comparison. The $Fe^{3+}/\sum Fe$ ratio also increases with magma evolution in this arc (Fig. 6C), and amphibole fractionation is occurring where Dy/Yb ratios decrease with elevated SiO_2 (Fig. 6D). In addition, the bulk composition of Kohistan arc is andesitic, which represents a paleo-intra-oceanic arc, and has affinity with continental crust (Tahirkheli et al., 1979; Jagoutz and Schmidt, 2012). We thus add the well-known Andean continental arc for comparison. As shown in Fig. 6E, the $Fe^{3+}/\sum Fe$ ratio of the Andean arc increases with decreasing Mg#, like in the Kohistan and Tonga arcs. The arc thickness (> 35 km) and scatter of Dy/Yb ratios may suggest that Andean arc magma experienced garnet fractionation, however the magnitude of the fractionation may be limited on the basis of the field evidence that hornblendite cumulates existed in the Andean arc root (e.g., Santana et al., 2020; Torres García et al., 2020), and the horizontal to slightly decreasing trends of Dy/Yb versus SiO_2 (Fig. 6F).

The formation of amphibole in the cumulates is attributed to either direct crystallization from parental liquids following the liquid line of descent (e.g., Dessimoz et al., 2012; Davidson et al., 2007) or peritectic reaction replacement with previously-crystallized clinopyroxene and/or olivine (e.g., Smith, 2014; Chang and Audétat 2018). Amphiboles in Kohistan cumulates are pargasites or tschermakites (Fig. S1). Our

observations show that they are mostly euhedral and that no residual clinopyroxene ± olivine is present (Fig. 2), which suggests that amphiboles in Kohistan amphibole-rich cumulates are crystallized directly from the magma. Since amphibole is the volumetrically abundant Fe-rich silicate phase, and Fe^{2+} occupies a greater proportion of C-sites in the amphibole relative to Fe^{3+}, as the $Fe^{3+}/\sum Fe$ ratios of amphibole decreases with magma evolution (Fig. 4), Fe^{3+} will be gradually enriched in residual melts. In addition, it should also be noted that the divergence of $Fe^{3+}/\sum Fe$ between bulk cumulates and amphiboles increases with the decrease of Mg#, which means that Fe-(Ti)-oxides may occur in the late-stage cumulates. Based on our observations there is rare magnetite and no ilmenite in the primitive (high Mg#) cumulates; the abundance of magnetite increases with the decreasing Mg#, but is still less than 1 vol.% in the low Mg# cumulates. Previous modeling shows that at high pressure (> 1 GPa), the magnetite will saturate when the oxygen fugacity is above FMQ (fayalite-magnetite-quartz buffer) (Tang et al., 2019a). These amphibole-bearing cumulates are formed under the pressure of 1.0 to 1.2 GPa (Jagoutz, 2014), indicating that the oxygen fugacities of these cumulates containing magnetite (low Mg#) are above FMQ. It is also supported by experimental studies that magnetite is the first oxide phase to appear on the liquidus when above the FMQ buffer (Toplis and Carroll, 1995).

Garnet is another Fe-rich phase in arc systems, and previous studies have suggested that the increasing oxidation state of evolved magmas in a thick continental crust is auto-oxidized and mainly controlled by fractionated magmatic garnets that have low $Fe^{3+}/\sum Fe$ ratios (0.04-0.08) (Tang et al., 2018, 2019a). Our results show garnets in

Kohistan cumulates also have low $Fe^{3+}/\sum Fe$ ratios (0.073-0.084). However, the $Fe^{3+}/\sum Fe$ ratios of garnet neither decrease with Mg# nor correlate with bulk cumulate compositions, therefore its fractionation cannot lead to progressive increases in the $Fe^{3+}/\sum Fe$ ratio of the residual melt.

In order to explore the relationship between amphibole and coexisting liquid, experimental run product data were compiled. Previous studies suggest that the Kohistan amphibole-bearing cumulates were fractionated from mantle-derived parental melts following a hydrous liquid line of descent (Jagoutz et al., 2011). Therefore, we selected the experiments where starting materials were basalt or high-Mg basaltic andesite, and water was saturated or near saturated. The results show that there is a strongly-correlative positive linear relationship between Mg# in amphibole (x) and in coexisting liquid (y) according to the equation of $y = 1.31064x^2 – 0.81394x + 0.39154$ (Fig. 7). In this case, amphiboles in Kohistan cumulates with Mg# between 0.7 and 0.47 would have coexisted with liquids with Mg# between 0.46 and 0.3; $Fe^{3+}/\sum Fe$ ratios of these liquids based on Fig. 6A have ratios of approximately 0.4 and 0.5, respectively. Using this relationship, the results are extrapolated to Tonga oceanic arc and Andean continental arc, giving $Fe^{3+}/\sum Fe$ ratios of residual melt of 0.4-0.45, and 0.5-0.6, respectively (Figs. 6D, F). It suggests that the coexisting liquid will likely have substantially higher $Fe^{3+}/\sum Fe$ ratios than the amphibole-bearing cumulates. Therefore, the fractionation of amphibole and the formation of amphibole-bearing cumulates in the deep crust would lead to an enrichment of the $Fe^{3+}/\sum Fe$ ratio in the residual melt.

To evaluate the effect quantitatively, we used a series of initial magma $Fe^{3+}/\sum Fe$

ratios and forward modeled the evolving trend of $Fe^{3+}/\sum Fe$ ratios of residual melts with cumulate fractionation. To improve robustness of models, the bulk $Fe^{3+}/\sum Fe$ of cumulates were recalculated on the basis of the $Fe^{3+}/\sum Fe$ of each mineral and their relative proportions (Table 1). The $Fe^{3+}/\sum Fe$ ratio of clinopyroxene is estimated on the basis of experimentally determined maximum Fe^{3+} partitioning between clinopyroxene and garnet (Purwin et al., 2013). Fig. 8 shows the residual melt $Fe^{3+}/\sum Fe$ as a function of the mass proportion of fractionated cumulate with different Mg#. The calculation curves indicate that the fractionation of cumulates with Mg# = 0.7 will increase the $Fe^{3+}/\sum Fe$ of residual melts when the initial melt $Fe^{3+}/\sum Fe$ exceeds 0.31. By contrast, when $Fe^{3+}/\sum Fe$ of the initial melt is below 0.31, the residual melts will evolve to be more reduced. In addition, the fractionation of late stage cumulates (Mg# = 0.47) will significantly and efficiently elevate the $Fe^{3+}/\sum Fe$ ratio of residual melts. In fact, the amphibole-bearing cumulate of Mg# = 0.7 coexists with the liquid of Mg# = 0.46, which indicates that the cumulate with Mg# = 0.7 is not the most primitive one. Therefore, the $Fe^{3+}/\sum Fe$ ratio of initial parental magmas must be less than 0.31, which is consistent with previously reported data ranges (Kelley and Cottrell, 2009; Lee, 2014). It also implies that the Kohistan amphibole-bearing cumulates fractionated from initial parental magma need an additional mechanism to acquire the $Fe^{3+}/\sum Fe$ values of the cumulates (0.3-0.4). Crystallization experiments conducted at 1.0 GPa show that the stability field of olivine, which prefers Fe^{2+}, is significantly expanded in hydrous magmas, resulting in an efficient increase of Fe^{3+} in residual melts (Ulmer et al., 2018). This makes olivine, also common in the lithospheric mantle zone of Kohistan arc, a

potential candidate for increasing the $Fe^{3+}/\sum Fe$ to 0.3-0.4 in the early stage of arc magma evolution. However, the filter effect of amphibole on the increase of $Fe^{3+}/\sum Fe$ of arc magma in the middle to late stage is undeniable.

Potential redox effect on arc magmas

The redox state of magma may be expressed by oxygen fugacity, although there is not really free oxygen inside the Earth. Rather, oxygen fugacity is the partial pressure of oxygen, which is an equivalent concept. It is the muti-valence elements in the magma that control the redox state of magma. Iron is, by mass, the most common multi-valence element on Earth, thus Fe-rich minerals are potential candidates for controlling magmatic redox. On the basis of this study, the fractionation of amphibole crystallized in deep crustal levels at high pressure may increase the $Fe^{3+}/\sum Fe$ ratio of coexisting liquid, meaning that it is an internal petrological factor driving magma oxidation (Fig. 9). A caveat in our redox budget model is that we assumed limited magnetite fractionation through much of the Fe-depleting calc-alkaline differentiation series. We suggest that magnetite, as an accessory mineral, has a limited effect on the $Fe^{3+}/\sum Fe$ ratio of residual melt. Indeed, the redox state of magma is influenced by many factors, and our study only provides a possible mechanism of an internal petrological factor (i.e. amphibole fractionation). Previous studies also suggest other crustal processes such as degassing or assimilation of oxidized material can lead to elevated oxygen fugacities (e.g., Burgisser and Scaillet, 2007; Humphreys et al., 2015; Lee et al., 2010). Water, as the most abundant volatile in subduction-zone magmas, is considered the key factor driving melt oxidation during degassing, but recent studies suggested that water

degassing has no effect on oxidation (Crabtree and Lange, 2012; Waters and Lange, 2016). In addition, studies of ultrasonic acoustic velocity measurements indicated that changes in pressure during magma upwelling have little effect on the oxygen fugacity (Kress and Carmichael, 1991), and a study of Kohistan arc suggested that there is no evidence for involvement of ancient crustal materials in their formation (Jagoutz and Schmidt, 2012). Therefore, to a large extent, the rise of $Fe^{3+}/\sum Fe$ ratio may truly reflect the increase of magma oxidation states (Fig. 9).

IMPLICATION

Amphibole, as a ubiquitous fractionating phase, is ubiquitous in both continental and island arcs. Our findings indicate that amphibole exerts a fundamental control on redox effect of middle to late stage arc magmas. $Fe^{3+}/\sum Fe$ ratios of amphibole decrease with cumulate Mg#, leading to increasing Fe^{3+} abundance in residual melts by multistage amphibole fractionation, i.e. accumulating in deep lower crust and potential fractional crystallization in a middle to shallow magma chamber. Porphyry copper deposits (PCDs) are closely associated with magmas with high oxidation state (Richards, 2003; Sillitoe, 2010). In oxidized conditions (ΔFMQ >1.5-2) of arc systems, sulfur is more likely to exist in the form of sulfate (SO_4^{2-}) over sulfide (S^{2-}), and dissolve in the silicate melt, which causes chalcophile elements, such as Cu, to remain in the melt (e.g., Richards, 2003; Sun et al., 2015). We propose that in addition to dehydration of subducted oceanic crust and sediments, amphibole fractionation also elevates the oxidation state of evolved magmas in subduction zones, which retain Cu in the residual

magma necessary to produce porphyry copper deposits. Considering the common occurrence of amphibole fractionation in arc crust (Davidson et al., 2007), this is probably a reliable mechanism for triggering porphyry copper deposit formation in subduction settings.

ACKNOWLEDGMENTS AND FUNDING

We thank Editor Callum Hetherington for handling the manuscript, providing insightful comments, and helping to polish its presentation. Constructive comments from Stephen Crabtree and three anonymous reviewers are appreciated. Andreas Audétat, Ming Tang, and Jia Chang are also gratefully acknowledged for discussion on early draft. We appreciate Junhu Wang and Rile Ge for their guidance in fitting Mössbauer spectral lines, Chenhao Luo for collecting data, and Xuesong Tong for Mössbauer spectroscopy discussion. This study is financially supported by National Natural Science Foundation of China (No. 41973037 and No. 41902062), and China Geological Survey Program (No. DD20201159).

REFERENCES CITED

Audétat, A., and Simon A.C. (2012) Magmatic controls on porphyry Cu genesis. In J.W. Hedenquist, M. Harris and F. Camus, Eds., Geology and genesis of major copper deposits and districts of the world: a tribute to Richard Sillitoe. Society of Economic Geologists, Special Publication, 16, 553-572.

Aulbach, S., Woodland, A.B., Vasilyev, P., Galvez, M.E., and Viljoen, K.S. (2017) Effect of low-pressure igneous processes and subduction on $Fe^{3+}/\sum Fe$ and redox state of mantle eclogites from Lace (Kaapvaal craton). Earth and Planetary Science Letters, 474, 283-295.

Bounce, M.N., Kelley, K.A., and Cottrell, E. (2014) Variations in $Fe^{3+}/\sum Fe$ of Mariana arc basalts and mantle wedge fO_2. Journal of Petrology, 55, 2513-2536.

Bucholz, C.E., and Kelemen, P.B. (2019) Oxygen fugacity at the base of the Talkeetna arc, Alaska. Contributions to Mineralogy and Petrology, 174, 79.

Burg, J.P. (2011) The Asia-Kohistan-India collision. In D. Brown and P.D. Ryan, Eds., Arc-Continent collision, p. 279-309. Springer.

Burgisser, A., and Scaillet, B. (2007) Redox evolution of a degassing magma rising to the surface. Nature, 445, 194-197.

Chang, J., and Audétat, A. (2018) Petrogenesis and metal content of hornblende-rich xenoliths from two Laramide-age magma systems in southwestern USA: Insight into the metal budget of arc magmas. Journal of Petrology, 59, 1869-1898.

Chen, K., Tang, M., Lee, C.T.A., Wang, Z.C., Zou, Z.Q., Hu, Z.C., and Liu, Y.S. (2020) Sulfide-bearing cumulates in deep continental arcs. The missing copper reservoir. Earth and Planetary Science Letters, 531, 115971.

Cottrell, E., and Kelley, K.A. (2011) The oxidation state of Fe in MORB glasses and the oxygen fugacity of the upper mantle. Earth and Planetary Science Letters, 305, 270-282.

Crabtree, S.M., and Lange, R.A. (2012) An evaluation of the effect of degassing on the oxidation state of hydrous andesite and dacite magmas: a comparison of pre- and post-eruptive Fe^{2+} concentrations. Contributions to Mineralogy and Petrology, 163, 209-224.

Davidson, J., Turner, S., Handley, H., Macpherson, C., and Dosseto, A. (2007) Amphibole “sponge” in arc crust? Geology, 35, 787-790.

De Hoog, J.C.M., Hattori, K.H., and Hoblitt, R.P. (2004) Oxidized sulfur-rich mafic magma at Mount Pinatubo, Philippines. Contributions to Mineralogy and Petrology, 146, 750-761.

Dessimoz, M., Müntener, O., and Ulmer, P. (2012) A case for hornblende dominated fractionation of arc magmas: the Chelan Complex (Washington Cascades). Contributions to Mineralogy and Petrology, 163, 567-589.

Dhuime, B., Bosch, D., Bodinier, J.L., Garrido, C.J., Bruguier, O., Hussain, S.S., and Dawood, H. (2007) Multistage evolution of the Jijal ultramafic-mafic complex (Kohistan, N Pakistan): Implications for building the roots of island arcs. Earth and Planetary Science Letters, 261, 179-200.

382 Erdman, M.E., Lee, C.T.A., Levander, A., and Jiang, H. (2016) Role of arc magmatism
383 and lower crustal foundering in controlling elevation history of the Nevadaplano
384 and Colorado Plateau: A case study of pyroxenitic lower crust from central Arizona,
385 USA. Earth and Planetary Science Letters, 439, 48-57.
386 Frost, D.J., and McCammon, C.A. (2008) The redox state of Earth's mantle. Annual
387 Review of Earth and Planetary Sciences, 36, 389-420.
388 Grove, T.L., Elkins-Tanton, L.T., Parman, S.W., Chatterjee, N., Müntener, O., and
389 Gaetani, G.A. (2003) Fractional crystallization and mantle-melting controls on
390 calc-alkaline differentiation trends. Contributions to Mineralogy and Petrology,
391 145, 515-533.
392 Humphreys, M.C.S., Brooker, R.A., Fraser, D.G., Burgisser, A., Mangan, M.T., and
393 McCammon, C. (2015) Coupled interactions between volatile activity and Fe
394 oxidation state during arc crustal processes. Journal of Petrology, 56, 795-814.
395 Jagoutz, O. (2010) Construction of the granitoid crust of an island arc part II: a
396 quantitative petrogenetic model. Contributions to Mineralogy and Petrology, 160,
397 359-381.
398 Jagoutz, O. (2014) Arc crustal differentiation mechanisms. Earth and Planetary Science
399 Letters, 396, 267-277.
400 Jagoutz, O., and Schmidt, M.W. (2012) The formation and bulk composition of modern
401 juvenile continental crust: The Kohistan arc. Chemical Geology, 298-299, 79-96.
402 Jagoutz, O., Müntener, O., Schmidt, M.W., and Burg, J.P. (2011) The role of flux- and
403 decompression melting and their respective fractionation lines for continental crust

formation: Evidence from Kohistan arc. Earth and Planetary Science Letters, 303, 25-36.

Jiang, Z.Q., Wang, Q., Li, Z.X., Wyman, D.A., Tang, G.J., Jia, X.H., and Yang, Y.H. (2012) Late Cretaceous (ca. 90 Ma) adakitic intrusive rocks in the Kelu area, Gangdese Belt (southern Tibet): Slab melting and implications for Cu-Au mineralization. Journal of Asian Earth Sciences, 53, 67-81.

Jogoutz, O., Burg, J.P., Hussain, S.S., Dawood, H., Pettke, T., Iizuka, T., and Maruyama, S. (2009) Construction of the granitoid crust of an island arc part I: geochronological and geochemical constraints from the plutonic Kohistan (NW Pakistan). Contributions to Mineralogy and Petrology, 158, 739-755.

Kelemen, P.B., Hanghøj, K., and Greene, A.R. (2014) 4.21-One view of the geochemistry of subduction-related magmatic arcs, with an emphasis on primitive andesite and lower crust. Treatise on Geochemistry (Second Edition), 4, 749-806.

Kelley, K.A., and Cottrell, E. (2009) Water and the oxidation state of subduction zone magmas. Science, 325, 605-607.

King, P.L., Hervig, R.L., Holloway, J.R., Delaney, J.S., and Dyar, M.D. (2000) Partitioning of Fe^{3+}/Fe_{total} between amphibole and basanitic melt as a function of oxygen fugacity. Earth and Planetary Science Letters, 178, 97-112.

Klencsár, Z., Kuzmann, E., and Vértes, A. (1996) User-friendly software for Mössbauer spectrum analysis. Journal of Radioanalytical and Nuclear Chemistry, 210, 105-118.

425 Kress, V.C., and Carmichael, I.S.E. (1991) The compressibility of silicate liquids
426 containing Fe_2O_3 and the effect of composition, temperature, oxygen fugacity and
427 pressure on their redox states. Contributions to Mineralogy and Petrology, 108,
428 82-92.
429 Lee, C.T.A. (2014) 4.12 – Physics and chemistry of deep continental crust recycling. In
430 H.D. Holland and K.K. Turekian, Eds., Treatise on Geochemistry, second edition.
431 Elsevier, Oxford, p. 423-456.
432 Lee, C.T.A., Luffi, P., Le Roux, V., Dasgupta, R., Albaréde, F., and Leeman, W.P. (2010)
433 The redox state of arc mantle using Zn/Fe systematics. Nature, 468, 681-685.
434 Ma, L., Wang, Q., Wyman, D.A., Jiang, Z.Q., Yang, J.H., Li, Q.L., Gou, G.N., and Guo,
435 H.F. (2013a) Late Cretaceous crustal growth in the Gangdese area, southern Tibet:
436 Petrological and Sr–Nd–Hf–O isotopic evidence from Zhengga diorite-
437 gabbro. Chemical Geology, 349-350, 54-70.
438 Ma, L., Wang, Q., Wyman, D.A., Li, Z.X., Jiang, Z.Q., Yang, J.H., Gou, G.N., and Guo,
439 H.F. (2013b) Late Cretaceous (100–89 Ma) magnesian charnockites with adakitic
440 affinities in the Milin area, eastern Gangdese: Partial melting of subducted oceanic
441 crust and implications for crustal growth in southern Tibet. Lithos, 175-176, 315-
442 332.
443 Melekhova, E., Blundy, J., Robertson, R., and Humphreys, M.C.S. (2015) Experimental
444 evidence for polybaric differentiation of primitive arc basalt beneath St. Vincent,
445 Lesser Antilles. Journal of Petrology, 56, 161-192.

446 Müntener, O., and Ulmer, P. (2018) Arc crust formation and differentiation constrained
447 by experimental petrology. American Journal of Science, 318, 64-89.
448 Nandedkar, R.H., Ulmer, P., and Müntener, O. (2014) Fractional crystallization of
449 primitive, hydrous arc magmas: an experimental study at 0.7 GPa. Contributions
450 to Mineralogy and Petrology, 167, 1015.
451 Purwin, H., Lauterbach, S., Brey, G.P., Woodland, A.B., and Kleebe, H.J. (2013) An
452 experimental study of the Fe oxidation states in garnet and clinopyroxene as a
453 function of temperature in the system $CaO–FeO–Fe_2O_3–MgO–Al_2O_3–SiO_2$:
454 implications for garnet–clinopyroxene geothermometry. Contributions to
455 Mineralogy and Petrology, 165, 623-639.
456 Richards, J.P. (2003) Tectono-magmatic precursors for porphyry Cu-(Mo-Au) deposit
457 formation. Economic Geology, 98, 1515-1533.
458 Richards, J.P. (2015) The oxidation state, and sulfur and Cu contents of arc magmas:
459 implication for metallogeny. Lithos, 233, 27-45.
460 Santana, L.C.V., McLeod, C.L., Blakemore, D., Shaulis, B., and Hill, T. (2020) Bolivian
461 hornblendite cumulates: Insights into the depths of Central Andean arc magmatic
462 systems. Lithos, 370-371, 105618.
463 Scheibner, C., and Speijer, R.P. (2008) Late Paleocene-early Eocene Tethyan carbonate
464 platform evolution—A response to long- and short-term paleoclimatic change.
465 Earth-Science Reviews, 90, 71-102.
466 Sillitoe, R.H. (2010) Porphyry copper system. Economic Geology, 105, 3-41.

Sun, W.D., Huang, R.F., Li, H., Hu, Y.B., Zhang, C.C., Sun, S.J., and Ling, M.X. (2015) Porphyry deposits and oxidized magmas. Ore Geology Reviews, 65, 97-131.

Tahirkheli, R.A.K., Mattauer, M., Proust, F., and Tapponnier, P. (1979) The India-Eurasia suture zone in northern Pakistan; synthesis and interpretation of recent data at plate scale. In F. Abul and K.A. DeJong, Eds., Geodynamics of Pakistan, p. 125-130. Geol. Surv. Pakistan, Quetta, Pakistan.

Tang, M., Erdman, M., Eldridge, G., and Lee, C.T.A. (2018) The redox "filter" beneath mgmatic orogens and the formation of continental crust. Science Advances, 4, 5.

Tang, M., Lee, C.T.A., Costin, G., and Höfer, H.E. (2019a) Recycling reduced iron at the base of magmatic orogens. Earth and Planetary Science Letters, 528, 115827.

Tang, Y.W., Chen, L., Zhao, Z.F., and Zheng, Y.F. (2019b) Geochemical evidence for the production of granitoids through reworking of the juvenile mafic arc crust in the Gangdese orogen, southern Tibet. Geological Society of America Bulletin, https://doi.org/10.1130/B35304.1

Toplis, M.J., and Carroll, M.R. (1995) An experimental study of the influence of oxygen fugacity on Fe-Ti oxide stability, phase relations, and mineral-melt equilibria in ferro-basaltic systems. Journal of Petrology, 36, 1137-1170.

Torres García, M.F., Calderón, M., Ramírez de Arellano, C., Hervé, F., Opitz, J., Theye, T., Fanning, C.M., Pankhurst, R.J., González-Guillot, M., Fuentes, F., and Babinski, M. (2020) Trace element composition of amphibole and petrogenesis of hornblendites and plutonic suites of Cretaceous magmatic arcs developed in the Fuegian Andes, southernmost South America. Lithos, 372-373, 105656.

Ulmer, P., Kaegi, R., and Müntener, O. (2018) Experimentally derived intermediate to silica-rich arc magmas by fractional and equilibrium crystallization at 1.0 GPa: an evalution of phase relationships, compositions, liquid lines of descent and oxygen fugacity. Journal of Petrology, 59, 11-58.

Waters, L.E., and Lange, R.A. (2016) No effect of H_2O degassing on the oxidation state of magmatic liquids. Earth and Planetary Science Letters, 447, 48-59.

Wen, D.R. (2007) The Gangdese batholith, southern Tibet: Ages, geochemical characteristics and petrogenesis, 120 p. Ph.D. dissertation, National Taiwan University.

Xu, W., Zhu, D.C., Wang, Q., Weinberg, R.F., Wang, R., Li, S.M., Zhang, L.L., Zhao, Z.D. (2019) Constructing the early Mesozoic Gangdese crust in southern Tibet by hornblende-dominated magmatic differentiation. Journal of Petrology, 60, 515-552.

Xu, W.C., Zhang, H.F., Luo, B.J., Guo, L., and Yang, H. (2015) Adakite-like geochemical signature produced by amphibole-dominated fractionation of arc magmas: An example from the Late Cretaceous magmatism in Gangdese belt, south Tibet. Lithos, 232, 197-210.

Zhang, J.B., Wang, R., Hong, J., Tang, M., and Zhu, D.C. (2021) Nb-Ta systematics of Kohistan and Gangdese arc lower crust: Implications for continental crust formation. Ore Geology Reviews, 133, 104131.

Zhang, Z.M., Zhao, G.C., Santosh, M., Wang, J.L., Dong, X., and Shen, K. (2010) Late Cretaceous charnockite with adakitic affinities from the Gangdese batholith,

511 southeastern Tibet: Evidence for Neo-Tethyan mid-ocean ridge
512 subduction? Gondwana Research, 17, 615-631.
513 Zheng, Y.C., Hou, Z.Q., Gong, Y.L., Liang, W., Sun, Q.Z., Zhang, S., Fu, Q., Huang,
514 K.X., Li, Q.Y., and Li, W. (2014) Petrogenesis of Cretaceous adakite-like
515 intrusions of the Gangdese Plutonic Belt, southern Tibet: Implications for mid-
516 ocean ridge subduction and crustal growth. Lithos, 190-191, 240-263.
517 Zhu, D.C., Wang, Q., Chung, S.L., Cawood, P.A., and Zhao, Z.D. (2019) Gangdese
518 magmatism in southern Tibet and India-Asia convergence since 120 Ma. In P.J.
519 Treloar and M.P. Searle, Ed., Himalayan Tectonics: A Modern Synthesis.
520 Geological Society, London, Special Publications, 483, doi: 10.1144/SP483.14.
521 Zhu, D.C., Zhao, Z.D., Pan, G.T., Lee, H.Y., Kang, Z.Q., Liao, Z.L., Wang, L, Q., Li,
522 G.M., Dong, G.C., and Liu, B. (2009) Early cretaceous subduction-related adakite-
523 like rocks of the Gangdese Belt, southern Tibet: Products of slab melting and
524 subsequent melt-peridotite interaction? Journal of Asian Earth Sciences, 34, 298-
525 309.
526

527 **Figure Captions:**

528 **Figure 1.** (A) Geological map of the Kohistan arc (modified from Jagoutz, 2014) (B)
529 A-B cross-section through the Indus valley from the Jijal Complex to the Sarangar
530 gabbro (after Dhuime et al., 2007).

531

532 **Figure 2.** Photomicrograph of Kohistan hornblendite (A), garnet hornblendite (B),
533 Tescan integrated mineral analyzer (TIMA) image of pyroxene garnetite (C), and
534 pyroxene garnetite (plane polarized light) (D). The yellow rectangle in C is the area of
535 D. Abbreviations: Amp-amphibole, Grt-garnet, Rt-rutile.

536

537 **Figure 3.** ^{57}Fe Mössbauer spectra of (A-D) garnet and (E-G) amphibole in Kohistan
538 cumulates.

539

540 **Figure 4.** $Fe^{3+}/\sum Fe$ vs. whole-rock Mg# of Kohistan cumulates, amphiboles in
541 cumulates, and garnets in cumulates. The dots are color-coded by volume percentage
542 of amphibole, which have an estimation error of ≤ 5 vol%. The $Fe^{3+}/\sum Fe$ values of
543 Kohistan cumulates were determined by wet chemistry method, those of amphiboles
544 and garnets were determined by Mössbauer spectroscopy.

545

546 **Figure 5.** (A) Mg# vs. SiO_2 and (B) FeO^T vs. MgO diagrams. Honshu, Luzon and
547 Kohistan-Ladakh arc magmas are from GEOROC database (http://georoc.mpch-
548 mainz.gwdg.de/georoc/Entry.html); Gangdese arc magmas are from Jiang et al. (2012),

549 Ma et al. (2013a, b), Tang et al. (2019b), Wen (2017), Xu et al. (2015), Zhang et al.
550 (2010), Zheng et al. (2014), Zhu et al. (2009); Kohistan cumulates are from Jagoutz and
551 Schmidt (2012); Arizona cumulates are from Chen et al. (2020).
552
553 **Figure 6.** Whole-rock $Fe^{3+}/\sum Fe$ ratios vs. Mg# and Dy/Yb ratios vs. SiO_2 of (A, B)
554 Kohistan arc, (C, D) Tonga arc and (E, F) Andean arc. The curves with arrows in A and
555 F are the fitting trendline. The highlighted dots in C and E are equal interval mean
556 values. The differentiation trends of Dy/Yb are from Davidson et al. (2007). The data
557 of the Tonga arc and Andean arc, and the $Fe^{3+}/\sum Fe$ ratios of the Kohistan arc, are from
558 the GEOROC database, and the Dy/Yb ratio data of the Kohistan arc are from Jagoutz
559 et al. (2013).
560
561 **Figure 7.** Relationship between the Mg# of coexisting liquid and the Mg# of
562 crystallized amphibole as suggested by experiments. The trendline equation and R-
563 squared value are displayed.
564
565 **Figure 8.** Residual melt $Fe^{3+}/\sum Fe$ values as a consequence of fractionating amphibole-
566 bearing cumulates from different initial parental magmas with different bulk cumulate
567 Mg#.
568
569 **Figure 9.** Schematic cross section of arc magma system and associated porphyry
570 deposit, showing the oxidation effect of amphibole fractionation in lower crustal

571 cumulates and potential shallow magma chamber within parentheses. The diagram is
572 modified from Audétat and Simon (2012).

Table 1 Major compositions and mode of the Kohistan cumulates.

Sample	Content (wt. %)											Mg#**	$Fe^{3+}/\Sigma Fe$***	Mode (vol. %)				
	SiO_2	TiO_2	Al_2O_3	$^{T}Fe_2O_3$	MnO	MgO	CaO	Na_2O	K_2O	P_2O_5	FeO*			Amp	Grt	Px	Pl	Mag
18JL015	43.32	1.12	13.88	11.00	0.14	15.33	12.82	2.19	0.21	0.01	6.50	0.74	0.34	100				
18JL016-1	40.61	0.87	16.81	15.56	0.23	12.63	12.78	0.48	0.03	0.01	9.10	0.62	0.35	30	50	20		
18JL016-2	42.81	0.53	16.59	14.20	0.35	13.85	10.78	0.82	0.08	0.01	7.90	0.66	0.38	30	50	20		
18JL017	48.37	0.69	19.45	12.37	0.20	5.73	10.84	2.21	0.07	0.06	7.60	0.48	0.32		40	60		<1
18JL019	42.75	0.24	16.74	14.51	0.43	13.93	11.18	0.21	0.00	0.00	8.50	0.66	0.35	5	60	35		trace
18JL020-1	43.24	1.35	14.83	11.59	0.10	15.05	11.42	2.27	0.15	0.01	7.20	0.72	0.31	80	20			
18JL020-2	43.43	1.34	14.43	11.54	0.10	15.08	11.58	2.31	0.18	0.01	6.60	0.72	0.36	80	20			
18JL021	41.88	0.33	17.27	17.32	0.42	11.08	11.36	0.32	0.00	0.01	12.50	0.56	0.20		70	30		trace
18JL022	43.05	1.30	14.80	12.75	0.15	13.22	12.69	1.90	0.12	0.01	6.60	0.67	0.42	20	60	20		
18JL023	41.95	1.22	17.16	11.46	0.08	13.52	11.71	2.74	0.16	0.01	6.50	0.70	0.37	85	15			
18JL025	50.72	0.73	18.53	12.14	0.24	5.37	9.79	2.21	0.17	0.10	7.20	0.47	0.34	10	50	30	10	trace
18JL026	47.64	0.87	18.91	13.34	0.23	5.92	11.51	1.35	0.08	0.15	8.15	0.47	0.32	40	30	30		trace
18JL028	52.20	0.82	18.23	11.27	0.20	4.65	9.73	2.60	0.18	0.14	7.20	0.45	0.29	10	60	10	10	
18JL029	40.42	1.78	16.32	15.30	0.13	12.00	11.21	2.57	0.25	0.02	8.85	0.61	0.36	80	20			
18JL030	44.18	1.16	11.99	13.31	0.18	10.43	17.39	1.25	0.09	0.02	7.05	0.61	0.41	65	35			
18JL031	41.67	1.27	16.53	13.38	0.11	12.61	11.58	2.63	0.20	0.02	7.55	0.65	0.37	80	20			
18JL032	43.51	0.78	17.98	15.60	0.30	8.29	12.52	0.99	0.01	0.03	11.40	0.52	0.19		60	40		
18JL033	45.41	1.40	18.11	12.83	0.20	6.55	13.33	1.98	0.18	0.02	7.95	0.51	0.31		60	40		
18JL035	51.87	0.61	18.14	10.90	0.19	5.60	10.34	2.17	0.13	0.05	8.35	0.51	0.15		70	20	10	<1
18JL040	46.70	0.93	18.96	13.86	0.24	6.08	11.43	1.46	0.09	0.24	7.95	0.47	0.36	30	30	30	10	<1

* FeO contents are determined by wet chemistry.

** Mg# = atomic [Mg/(Mg+Fe)].

*** $Fe^{3+}/\Sigma Fe$ = atomic $[Fe^{3+}/(Fe^{3+}+Fe^{2+})]$, $Fe_2O_3 = {}^{T}Fe_2O_3 - FeO/0.8998$.

Abbreviations: Amp-amphibole, Grt-garnet, Px-pyroxene, Pl-plagioclase, Mag-magnetite.

Figure 1

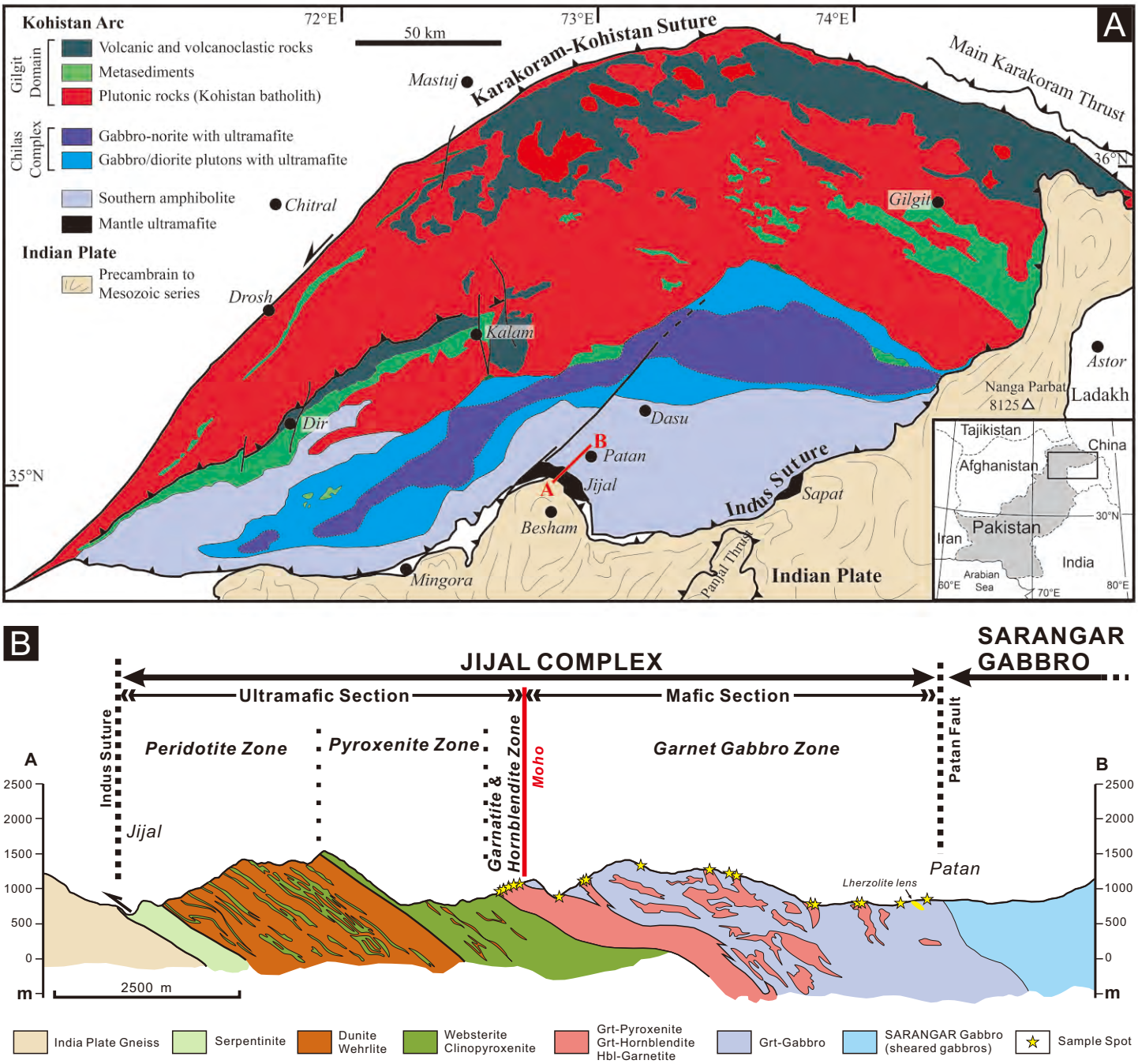
A
Kohistan Arc
Gilgit Domain
Volcanic and volcanoclastic rocks
Metasediments
Plutonic rocks (Kohistan batholith)
Chilas Complex
Gabbro-norite with ultramafite
Gabbro/diorite plutons with ultramafite
Southern amphibolite
Mantle ultramafite
Indian Plate
Precambrain to Mesozoic series
72°E
73°E
74°E
50 km
35°N
36°N
Karakoram-Kohistan Suture
Main Karakoram Thrust
Indus Suture
Panjal Thrust
Mastuj
Chitral
Drosh
Dir
Kalam
Gilgit
Astor
Nanga Parbat 8125
Ladakh
Dasu
Patan
Jijal
Sapat
Besham
Mingora
Indian Plate
Tajikistan
China
Afghanistan
Pakistan
Iran
India
Arabian Sea
30°N
60°E
70°E
80°E
B
JIJAL COMPLEX
SARANGAR GABBRO
Ultramafic Section
Mafic Section
Peridotite Zone
Pyroxenite Zone
Garnatite & Hornblendite Zone
Moho
Garnet Gabbro Zone
Indus Suture
Patan Fault
A
B
Jijal
Patan
Lherzolite lens
2500
2000
1500
1000
500
0
m
2500 m
India Plate Gneiss
Serpentinite
Dunite Wehrlite
Websterite Clinopyroxenite
Grt-Pyroxenite Grt-Hornblendite Hbl-Garnetite
Grt-Gabbro
SARANGAR Gabbro (sheared gabbros)
Sample Spot

Figure 2

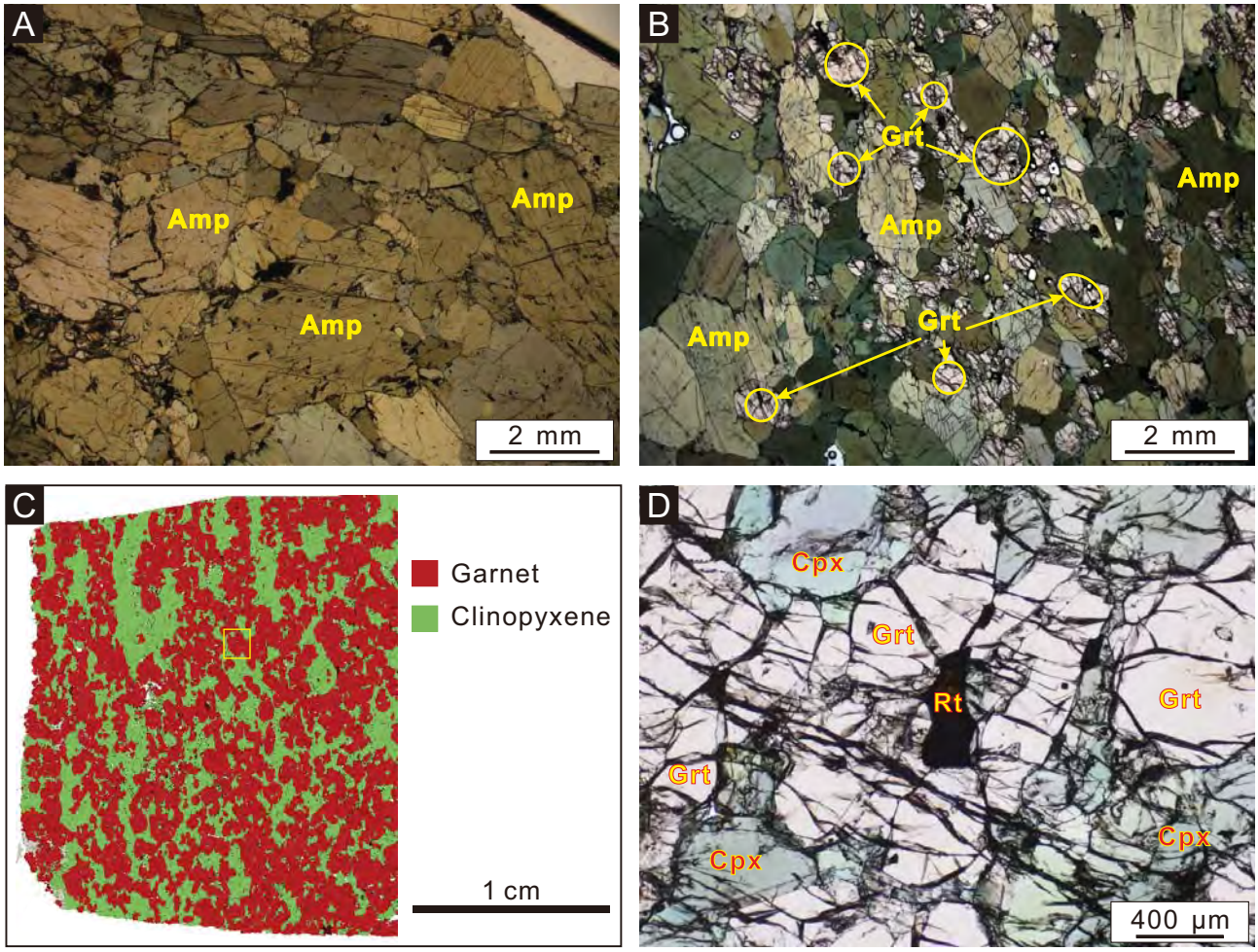
A
Amp
Amp
Amp
2 mm
B
Grt
Amp
Amp
Amp
Grt
2 mm
C
Garnet
Clinopyxene
1 cm
D
Cpx
Grt
Rt
Grt
Grt
Cpx
Cpx
400 μm

Figure 3

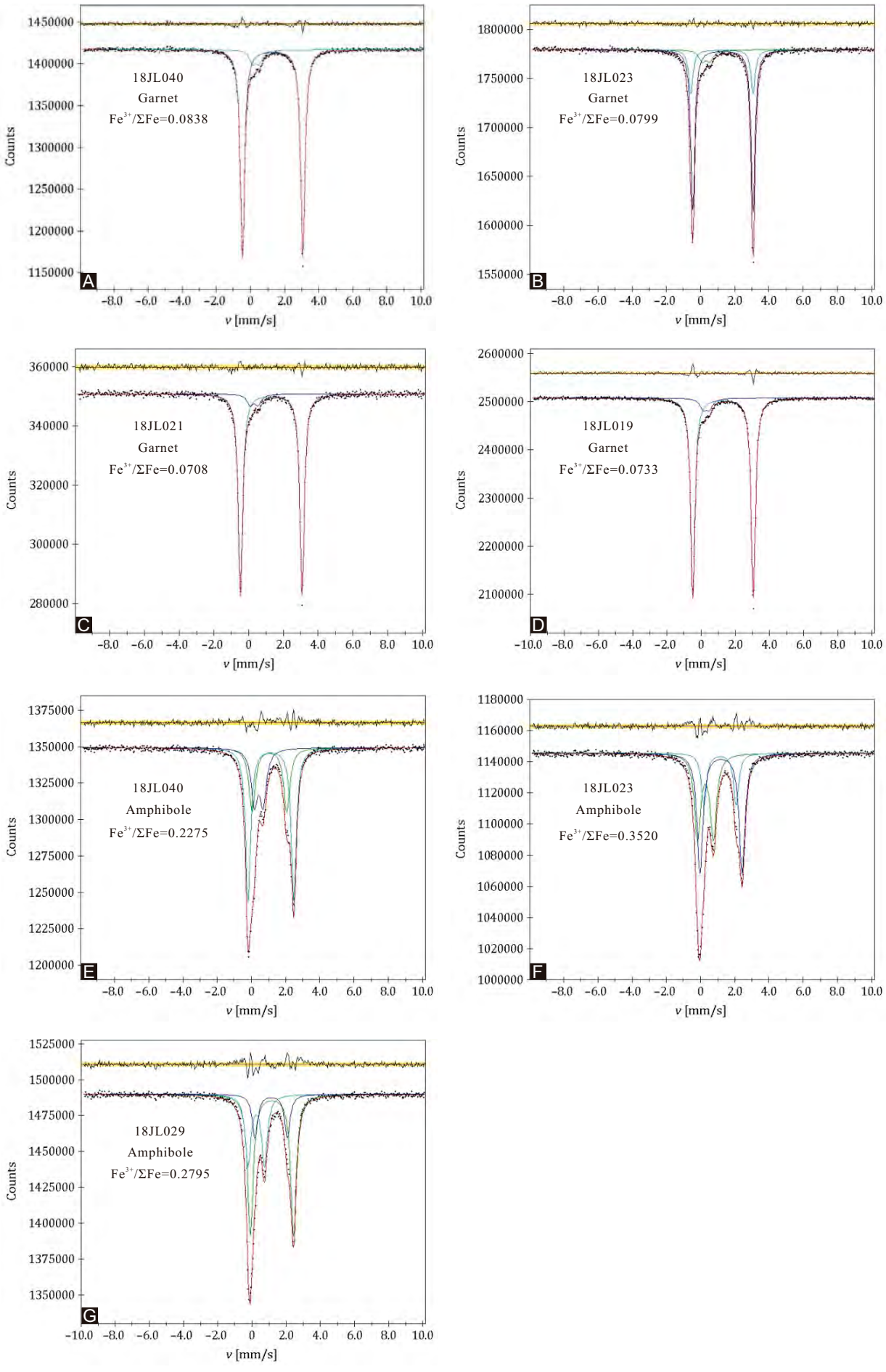
18JL040
Garnet
Fe3+/ΣFe=0.0838
A
18JL023
Garnet
Fe3+/ΣFe=0.0799
B
18JL021
Garnet
Fe3+/ΣFe=0.0708
C
18JL019
Garnet
Fe3+/ΣFe=0.0733
D
18JL040
Amphibole
Fe3+/ΣFe=0.2275
E
18JL023
Amphibole
Fe3+/ΣFe=0.3520
F
18JL029
Amphibole
Fe3+/ΣFe=0.2795
G
Counts
v [mm/s]

Figure 4

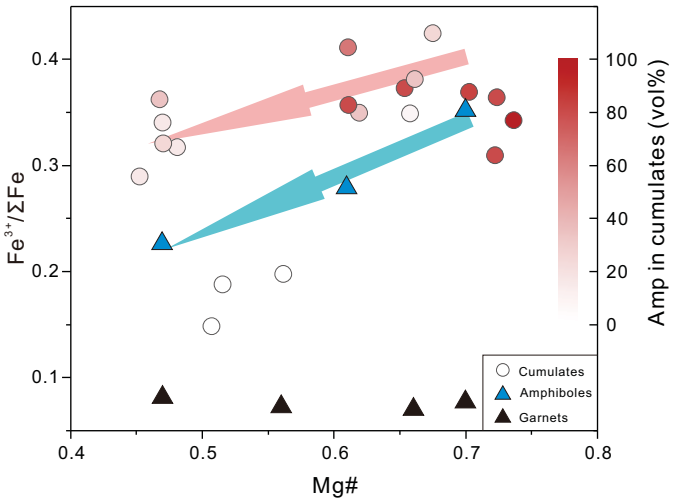
0.4
0.3
0.2
0.1
Fe3+/ΣFe
0.4
0.5
0.6
0.7
0.8
Mg#
100
80
60
40
20
0
Amp in cumulates (vol%)
Cumulates
Amphiboles
Garnets

Figure 5

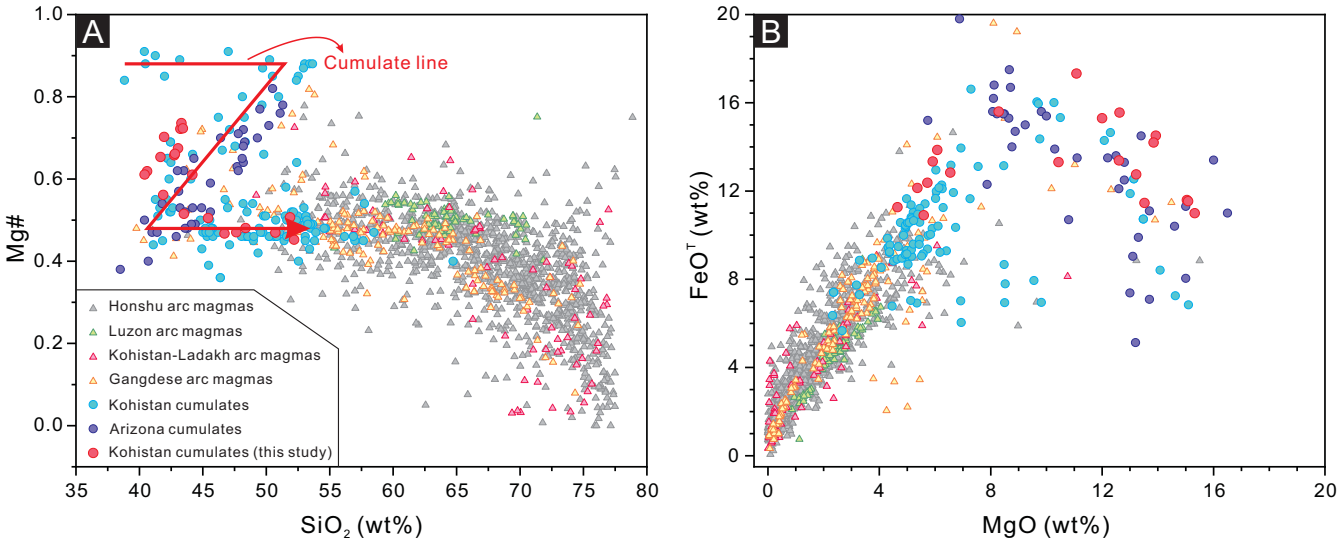
A
Cumulate line
Mg#
SiO2 (wt%)
Honshu arc magmas
Luzon arc magmas
Kohistan-Ladakh arc magmas
Gangdese arc magmas
Kohistan cumulates
Arizona cumulates
Kohistan cumulates (this study)
B
FeOT (wt%)
MgO (wt%)

Figure 6

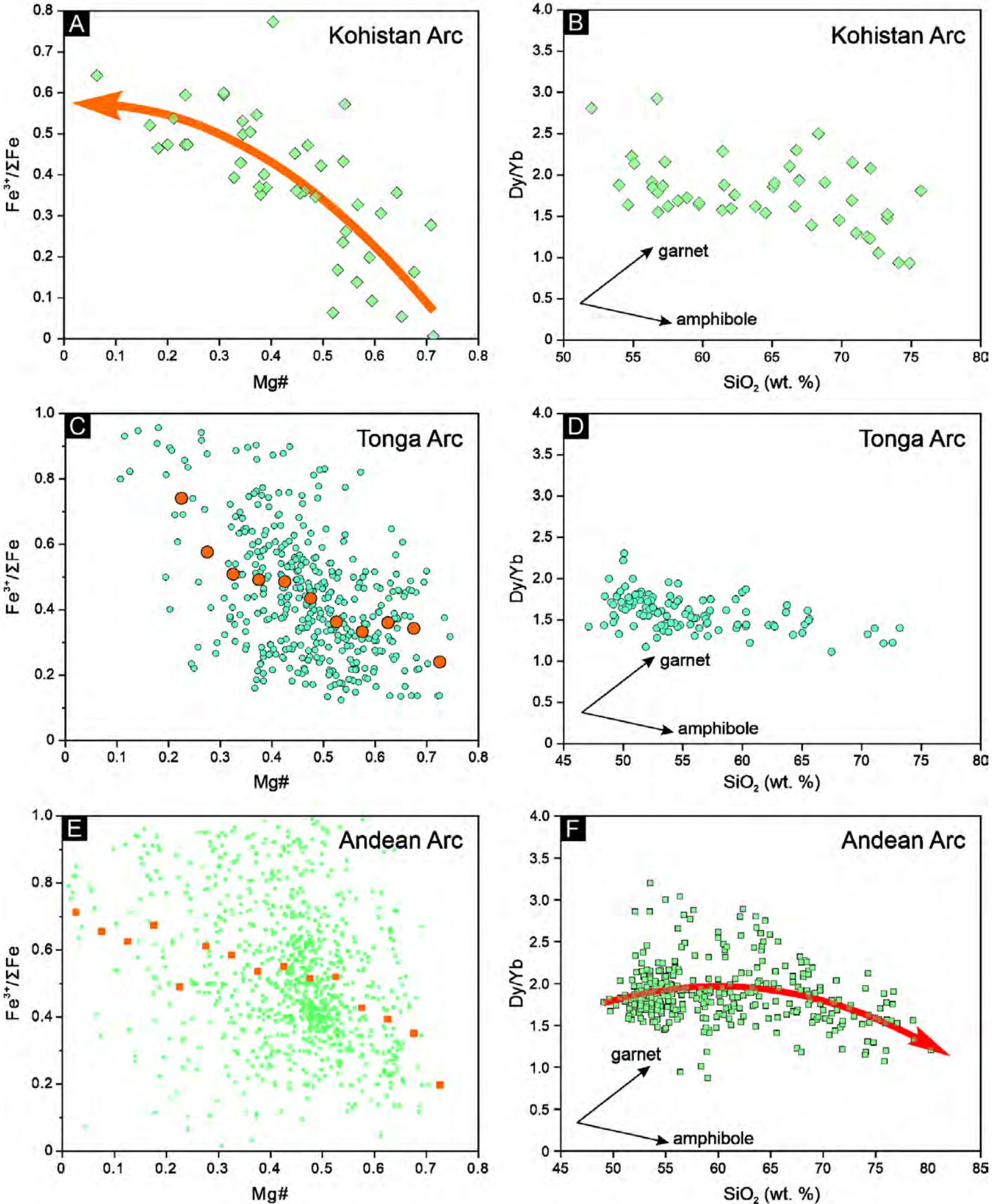
A
Kohistan Arc
Fe3+/ΣFe
Mg#
B
Kohistan Arc
Dy/Yb
garnet
amphibole
SiO2 (wt. %)
C
Tonga Arc
Fe3+/ΣFe
Mg#
D
Tonga Arc
Dy/Yb
garnet
amphibole
SiO2 (wt. %)
E
Andean Arc
Fe3+/ΣFe
Mg#
F
Andean Arc
Dy/Yb
garnet
amphibole
SiO2 (wt. %)

Figure 7

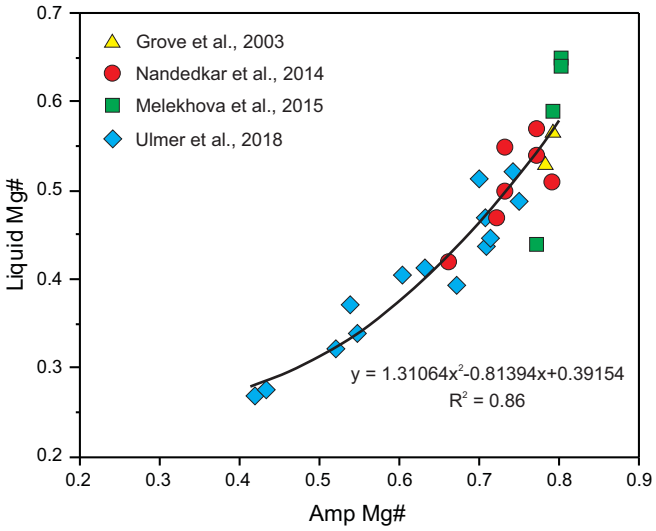
Grove et al., 2003
Nandedkar et al., 2014
Melekhova et al., 2015
Ulmer et al., 2018
y = 1.31064x²-0.81394x+0.39154
R² = 0.86
Liquid Mg#
Amp Mg#
0.2
0.3
0.4
0.5
0.6
0.7
0.8
0.9

Figure 8

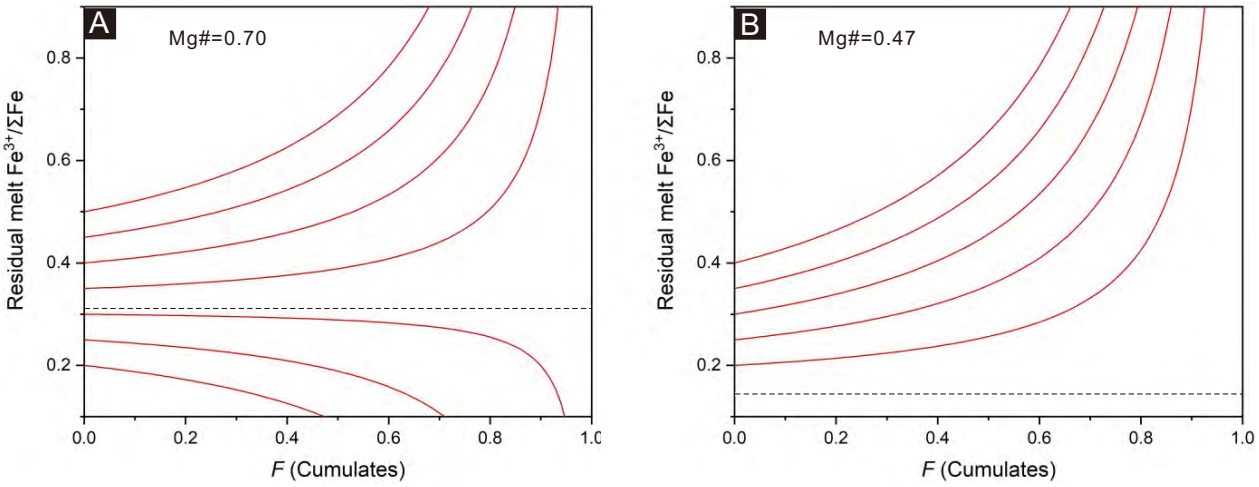
A
Mg#=0.70
B
Mg#=0.47
Residual melt Fe3+/ΣFe
F (Cumulates)
0.0
0.2
0.4
0.6
0.8
1.0

Figure 9

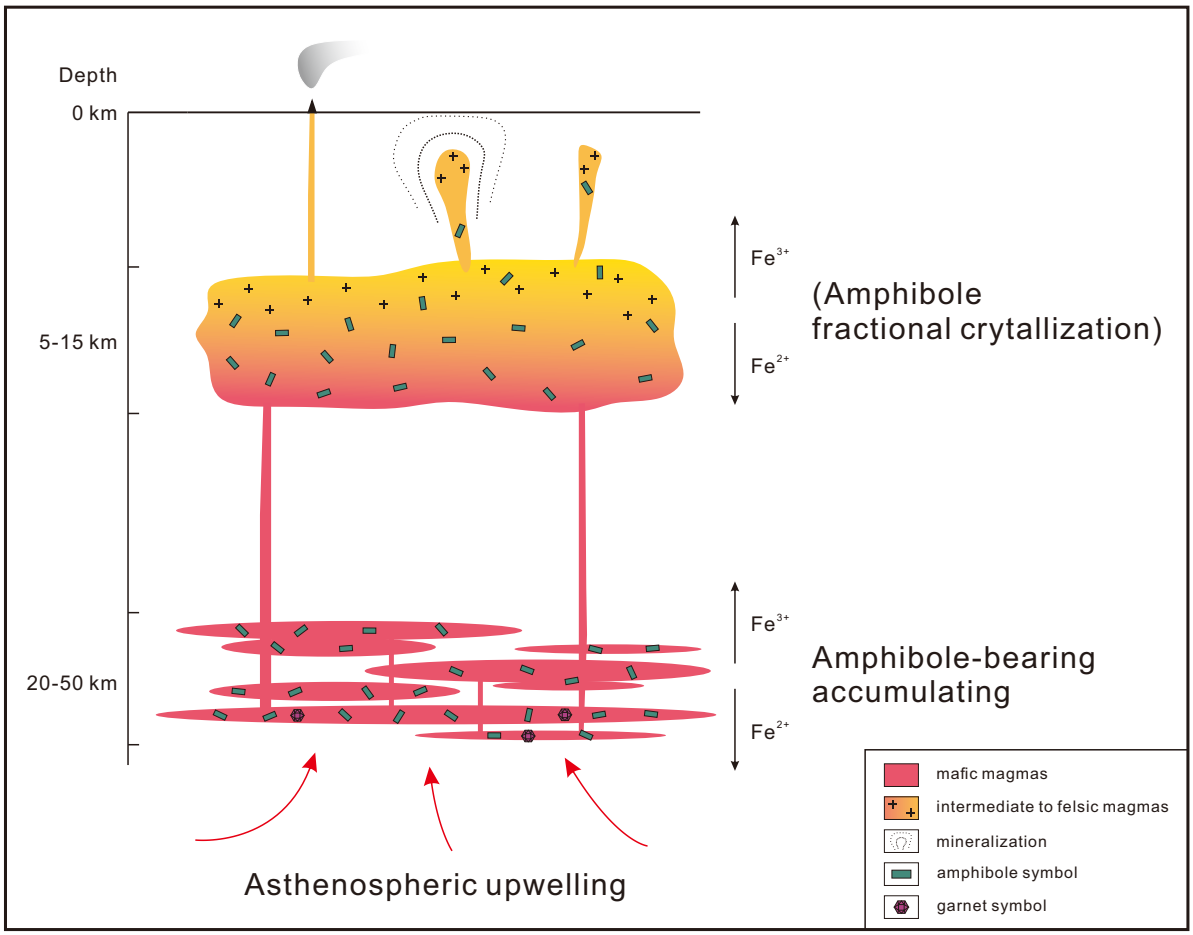
Depth
0 km
5-15 km
20-50 km
Fe3+
Fe2+
(Amphibole
fractional crytallization)
Fe3+
Fe2+
Amphibole-bearing
accumulating
Asthenospheric upwelling
mafic magmas
intermediate to felsic magmas
mineralization
amphibole symbol
garnet symbol